Structure, density, and velocity fluctuations in quasi-two-dimensional non-Brownian suspensions of spheres

F. Rouyer
Laboratoire Fluides Automatique et Systémes Thermiques, Universités P. et M. Curie et Paris Sud, C.N.R.S. (UMR 7608), Bâtiment 502, Campus Universitaire, 91405 Orsay Cedex, France

D. Lhuillier
Laboratoire de Modélisation en Mécanique, Université P. et M. Curie, C.N.R.S. (UMR 7606), 75252 Paris Cedex 05, France

J. Martin and D. Salin[a)]
Laboratoire Fluides Automatique et Systémes Thermiques, Universités P. et M. Curie et Paris Sud, C.N.R.S. (UMR 7608), Bâtiment 502, Campus Universitaire, 91405 Orsay Cedex, France

Non-Brownian sedimenting suspensions exhibit density and velocity fluctuations. We have performed experiments on a quasi-two-dimensional counter-flow stabilized suspension of 2000 spherical particles, namely a liquid–solid fluidized bed in a Hele–Shaw cell. This two-dimensional suspension displays a uniform concentration but the particle radial distribution function and the fluctuations of the particle number in a subvolume of the suspension suggest that the microstructure is far from being random. We have also measured the velocity fluctuations of a test particle and the fluctuations of the mean particle velocity in a subvolume. It happens that the relation between velocity and concentration fluctuations in a subvolume can be deduced from a balance between buoyancy and parietal friction forces. © *2000 American Institute of Physics.* [S1070-6631(00)02305-9]

I. INTRODUCTION

The hydrodynamics of a noncolloidal suspension of monodisperse spherical particles in a viscous liquid is still an open problem. In the presence of gravity, each particle settles, but as a result of its hydrodynamic interactions with the other particles, it settles with a time-dependent velocity.[1–6] The average velocity and the mean square velocity fluctuations depend (at least) on the two-particle distribution function.[7–9] This spatial distribution has been generally supposed to be that of a random suspension, i.e., all correlations between particles' positions are usually neglected, except those resulting from the hard-sphere interactions.[5,8–10] A consequence of this assumed random distribution is the increase of the particles' density or velocity fluctuations with the size of the container,[5,8,9] in contradiction with experiments on fluidized beds[11] and sedimenting suspensions.[12] However, recent experiments on very dilute experiments[6] showed a size dependence, ending with some saturation of the velocity fluctuations for large enough containers. Moreover, recent improvements in nuclear magnetic resonance techniques[13] have allowed one to deduce the structure factor $S(k)$ of a sedimenting suspension, and this was not a random one. Therefore knowledge of the microstructure is required. A very special nonrandom microstructure[14] was tentatively used to account for the saturation of particle velocity fluctuations. An alternative explanation, based on real suspensions which are bounded by walls, takes into account a de-

tailed analysis of the role of the boundaries.[15] Which is the relevant answer is still an open question to be addressed in the three-dimensional (3-D) suspension, and we do not pretend to solve that controversial issue.

Instead, we focus on an apparently much simpler case for which the microstructure and the velocity fluctuations can be thoroughly measured. For that purpose, we use our ''favorite'' counterflow stabilized suspension,[3] namely a liquid–solid fluidized bed, to address the concentration-dependent structure of the suspension, as well as the related density and velocity fluctuations. We have designed a two-dimensional (2-D) fluidized bed, by imposing a constant upward flow in a Hele–Shaw cell (HS), consisting of two parallel plates, separated by a small gap, just slightly larger than the sphere diameter. This setup allows us to easily reach a steady state and enables us to get reliable and extensive data for all particles involved. Using direct videoscopy of the 2000 particles, we record their positions, trajectories, and velocities, from which we determine the spatial distribution function $g(r)$, the particles' velocity fluctuations δu_p as well as the particles number fluctuations ΔN_R and mean velocity fluctuations ΔU_R versus the size of the volume of measurement, v_R, a disk of radius R.

II. EXPERIMENTAL SETUP

The HS cell consists of two parallel glass plates of length 80 cm and width 10 cm, separated by a uniform spacer which ensures a constant gap of thickness $b=2.0$ mm. The thickness of each plate (1 cm) is large enough to avoid

---

[a)]Electronic mail: dos@fast.u-psud.fr

bending. The cell is held vertically along the larger dimension. The monodisperse spherical particles are 2000 roller bearings made of brass or aluminum (density 8.7 or 2.7) with a diameter $2a = 1.50$ mm, just slightly smaller than the cell gap b. We use water-glycerin mixtures of viscosity around $\eta = 0.4$ Pa s and density 1.25. At such conditions, the sedimentation velocity is $U_s \sim 6$ mm s^{-1}, hence the corresponding Reynolds number, Re$= aU_s/\nu$, is always smaller than 10^{-1}. Contrary to gas-fluidized beds, which are usually unstable, a liquid-fluidized bed is stable for these low Re.[3] At the bottom inlet of the HS cell, the bed is supported by a porous filter which ensures uniform injection. Experiments are performed at constant upward flow rates using overfilled inlet and outlet vessels at different heights. In such a 2-D fluidized bed, the effective volume fraction, $\phi_{2\text{-D}}$, can be related to the surface fraction, $C = \rho \pi a^2$ (ρ is the number of particles per unit area), through $\phi_{2\text{-D}} = 4Ca/3b = C/2$. The upward fluid filtration velocity, U_d, controls the bed expansion, namely the concentration. At low flow rates, the bed is close packed whereas a flow rate above the minimum fluidization velocity results in a uniform expansion of the bed from top to bottom, such that the larger U_d, the smaller the concentration. A steady state is achieved within 10 min; this time is typically 100 times the time needed by a particle to go through the thickness of the cell, and more than 10 times the time needed by the suspension in sedimentation to settle down the bottom of the cell. Our data on the filtration velocity versus concentration are coincidentally found to obey a Richardson–Zaki law $U_d \sim U_s(1 - \phi_{2\text{-D}})^5$, with an exponent close to that of 3-D fluidized beds.[3,11] Using our technique, we have been able to vary C from 8% to 76%. Below 8%, the bed starts ''flowing'' to the top of the cell as the fluid velocity experienced by the particles in the middle of the gap becomes larger than the single particle sedimentation velocity between two plates U_s. For this reason, our system is not suitable for measurements at very low concentrations. At the 2-D maximum close packing, we get $C \sim 80\%$, which is close to the maximum packing of well-arranged disks.[16]

The whole bed is illuminated and a charge-coupled device video-tape camera records the movements of the 2000 particles. Each image is digitized and the position of the centers of all particles is recorded using the NIH IMAGE software. By tracking the particles between consecutive frames, we can record their positions, their trajectories, and compute their instantaneous velocities. The typical accuracy of our measurements is 0.1 mm in position and 5% in velocity. Figure 1 shows snapshots of the positions of the particles and their velocities. The particles are in permanent motion, participating from time to time in the formation of doublets, triplets, clusters, etc., then separating to form similar temporary structures with other particles.

III. STRUCTURE AND DENSITY FLUCTUATIONS

In this section, we determine the pair distribution function $g(\mathbf{r})$ and calculate the long wavelength structure factor at various concentrations. We also compare the thermodynamics of this new fluid-like suspension to the one of a hard-disk (HD) system[17,18] and analyze its salient features.
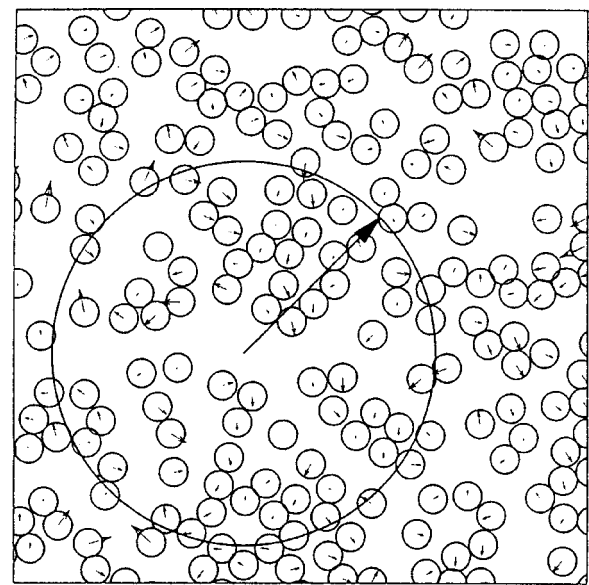

FIG. 1. Snapshots of particle positions and instantaneous velocities at area fractions 35%, in a window of 30×30 mm^2 located in the middle of the cell. The vertical is along the gravity direction. The circle is our R-dependent area of measurement.

A. Pair distribution function

The 2-D pair distribution function $g(\mathbf{r})$ is related to the probability of observing a particle centered at $\mathbf{r}$, provided a test particle is already centered at the origin. This function is defined through

$$g(\mathbf{r}) = \left\langle \frac{A}{N^2} \sum_{i=1}^{N} \sum_{j \neq i=1}^{N} \delta(\mathbf{r} - \mathbf{r_{ij}}) \right\rangle, \qquad (1)$$

where N is the total number of particles in area A. To evaluate $g(\mathbf{r})$, we choose a test particle on a snapshot, and count the number of particles centered in a small volume around $\mathbf{r}$. Since our suspension was checked to have a homogeneous concentration, we can use several test particles on the same snapshot. Afterwards, we use different snapshots (~ 50) taken at different times and we perform the average. No anisotropy along the vertical (z, i.e., the sedimenting direction) or the horizontal (x) direction, could be detected. Indeed, in Fig. 1, the vertical direction can hardly be guessed. Then, the relevant distribution function is the radial pair distribution function (RDF), $g(r) = g(|\mathbf{r}|)$. It is plotted in Fig. 2 versus the normalized distance $r/2a$ between sphere centers, for different concentrations. The occurrence of correlations for values smaller than $2a$ can be attributed to the overlapping of particles within the gap of the cell ($r_{\min} = 1.42$ mm); the larger b, the larger the overlapping (our choice of b is a compromise between friction and overlapping). There is evidence of a strong tendency for particles to be close to one another, whereas at large distances the structure is random (of equal probability). We note that as the concentration increases, the RDF acquires more structure: The maxima and minima, respectively, located around $r = 2a, 4a, 6a$ and $3a, 5a, 7a$, become more and more contrasted. These features are reminiscent of hard-disk and hard-sphere liquids[18,19] and were also observed in simulations[5] of the structure factor.
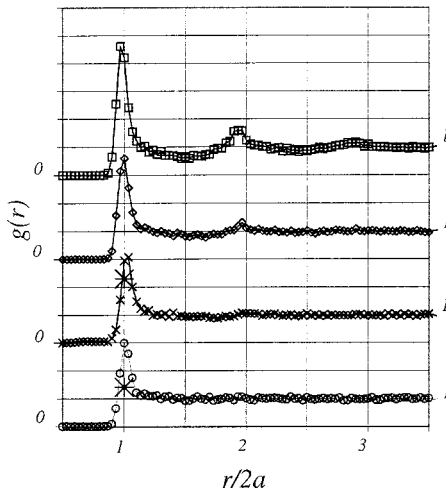
FIG. 2. Radial pair distribution function $g(r)$ vs the reduced distance $r/2a$, at various area concentrations (in %): $C=21$ ($\bigcirc$), 28 ($\times$), 46 ($\diamond$), 70 ($\square$). For clarity the curves are shifted vertically by a constant value [note that $g(0)=0$ and $g(\infty)=1$ in all cases].

Compared to a monoatomic liquid, these maxima do not shift with the density of the fluid, and are always obtained for r values multiple of $2a$. A quantitative comparison with HD fluid is illustrated in Fig. 2, where the large stars correspond to the maximum value of the RDF of HD fluid for $r=2a$ for two relatively low concentrations. This maximum can be calculated only before freezing, i.e., for concentration less than $C^* \sim 49\%$ for which a steady configuration of hard disk in equilibrium can be obtained.[17] Compared to a randomly distributed HD fluid, we note here the formation of many more doublets, triplets, etc. Especially at low concentrations, we measure $g(r=2a) \sim 3$, whereas for a low concentration HD fluid $g(r=2a) \sim 1$. The comparison of measured RDF with HD ones clearly shows that our quasi-2-D suspension is not random. This feature is inherent to hydrodynamic interactions: the particles arrange themselves close to each other in order to minimize the viscous dissipation in the fluid.

Before calculating the structure factor of the suspension, let us first recall some definitions of statistical physics. We define the mean square number of particles in a disk of radius R:

$$\overline{N_R^2} = \int_{r,r' \leqslant R} \overline{\rho(r)\rho(r')} d\mathbf{r} \, d\mathbf{r}', \tag{2}$$

where $\rho(r)$ is the probability density to have a particle centered at r. Equation (2) can be rewritten in case of homogeneity:

$$\overline{N_R^2} = \overline{N_R}\left[1 + \rho \int_{r \leqslant R} g(r) d\mathbf{r}\right], \tag{3}$$

where $\rho = N/A = C/\pi a^2$ is the number density. Thus, the standard deviation of N can be written:

$$\Delta N_R^2 = \overline{N_R^2} - \overline{N_R}^2 = \overline{N_R}\left[1 + \rho \int_{r \leqslant R} (g(r)-1) d\mathbf{r}\right]. \tag{4}$$
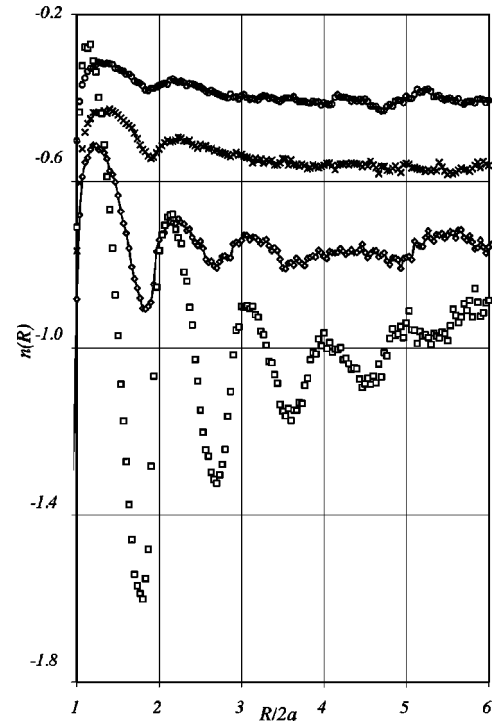

FIG. 3. The integrated pair correlation function, $n(R)$ [Eq. (7)] plotted vs the reduced distance from a test sphere $R/2a$ for the same concentrations as in Fig. 2.

B. Long-wave structure factor

The long wavelength (zero wave number) structure factor, $S_0(C)$, is a function of the concentration C of the suspension, and is defined as

$$S_0(C) = \lim_{R \to \infty}\left[1 + \rho \int_{r \leqslant R} (g(r)-1) 2\pi r \, dr\right]. \tag{5}$$

For an homogeneous system we get from Eq. (4) the usual relation:

$$S_0(C) = \lim_{R \to \infty}\left[\frac{\Delta N_R^2}{\overline{N_R}}\right]. \tag{6}$$

According to Eq. (5), we can determine $S_0(C)$ from integration of the pair correlation over a disk $r \leqslant R$ where R is a mesoscopic distance (much larger than the particle diameter but smaller than the width of our suspension, here $R < 5$ cm). The relevant quantity,

$$n(R) = \rho \int_{r \leqslant R} (g(r)-1) d\mathbf{r}, \tag{7}$$

also called mass deficit,[5,14] has been computed with our RDF and is plotted in Fig. 3 as a function of the reduced distance. We observe that above a distance $\sim 10a$ the curves approach a concentration-dependent plateau $n(\infty)$. As C tends to the packing fraction, the plateau tends toward -1. A concentration decrease results in larger values of the plateau, which reaches -0.2 for our lower concentration $C=8\%$. Note that these results disagree with the Koch and Shaqfeh theory for 3-D suspensions[14] which conjectured, to account for velocity fluctuations independent of the vessel size, a particular dis-

Phys. Fluids, Vol. 12, No. 5, May 2000

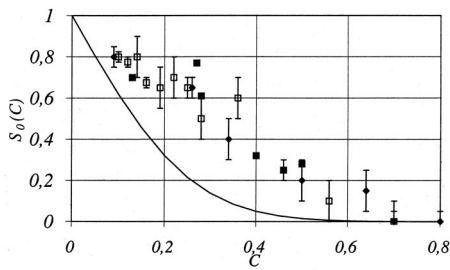Structure, density, and velocity fluctuations in suspensions   961

FIG. 4. The structure factor vs concentration computed from $g(r)$ [Eq. (5)] for brass ($\square$) and aluminum ($\blacklozenge$) spheres, and from $\Delta N_R^2/N_R$ [Eq. (6)] for brass ($\bullet$) spheres. The full line is the theoretical structure factor for a random distribution of hard disk.

FIG. 6. Single particle velocity fluctuations u_0 normalized by U_d vs C. Closed and open symbols correspond, respectively, to the horizontal and vertical velocity fluctuations (δu_x and δu_z), to aluminum beads ($\square$), to brass beads for a cell's width of 10 cm ($\triangle$), and to brass beads in a larger cell ($\bigcirc$) (20 cm).

tribution of the centers of particles, resulting in a complete screening of the hydrodynamic interactions. Thus, this particular distribution had to be such that $n(\infty) = -1$ whatever the concentration is. On the other hand, our results agree with Ladd's numerical simulation of 3-D suspensions without walls, in which partial screening was obtained.[5] But we insist that our results concern a 2-D suspension primarily.

As $n(R)$ reaches a constant values for $R \gtrsim 10a$, we can obtain $S_0 = 1 + n(\infty)$, which is plotted in Fig. 4 as a function of concentration. For comparison, we recall that in a perfect gas, for which $g(r) = 1$, $S_0(0) = 1$: The fluctuations are equal to the square root of the number of particles. In a solid which is incompressible, at zero temperature, $S_0(C^*) = 0$: There are no fluctuations of the particle density. For a quantitative comparison of our results with HD model, we plot as a dashed line in Fig. 4 the corresponding HD's $S_0(C)$.[18] Once again our data cannot be described by the HD fluid: Our 2-D suspension is definitively not a random system. In most 3-D suspension theories, a Percus–Yevick hard-sphere RDF is assumed, that is a random distribution of the centers of particles in suspension. Our 2-D data as well as 3-D nuclear magnetic resonance measurements,[13] therefore suggest that the hypothesis of randomness should be addressed.

C. Fluctuations in a subvolume

One could object that the integration over the disk $r \leq R$ could lead to an enhancement of the experimental errors on $g(r)$, and then to a poor estimation of $S_0(C)$. In fact, there is an independent way to check the result by measuring the fluctuations of the number N_R of particles with centers inside a disk of radius R [cf. Eq. (6)]. From our data, we can
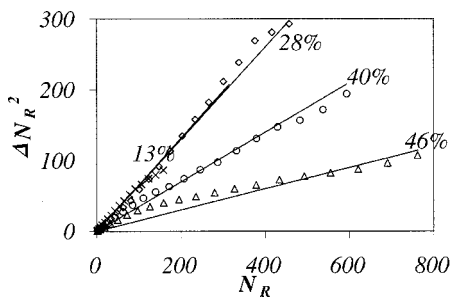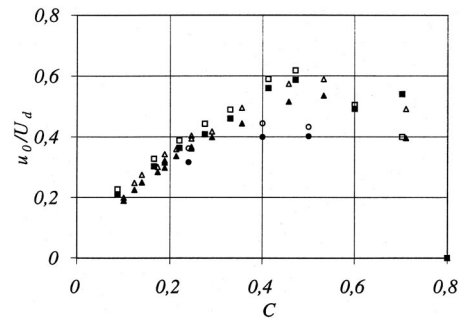

FIG. 5. $\Delta N_R^2(R)$ vs $N_R(R)$ for $C = 13$ ($\times$), 28 ($\diamond$), 40 ($\bigcirc$), $46(\triangle)\%$. The line through the data gives the structure factor $S(C)$.

easily measure N_R and the averages $\overline{N_R}$ and $\overline{N_R^2}$. For that purpose, we count the particles in areas πR^2 randomly located over the cell, and we average the data over many snapshots (typically 200), these snapshots being randomly chosen on a movie of at least 7 min. Before averaging over the different locations, we have checked the homogeneity of the suspension through the proportionality between $\overline{N_R}$ and R^2: All the plots display a slope of C/a^2 for each selected location. Figure 5 is a plot of ΔN_R^2 vs N_R. A linear dependence is obtained for all concentrations up to approximately 50%. According to Eq. (5), the proportionality coefficient between ΔN_R^2 and $\overline{N_R}$ gives the structure factor $S_0(C)$. For the larger concentrations, the local structure of the suspension increases the range of $g(r)$ beyond our accessible range of R and the relation between ΔN_R and $\overline{N_R}$ is less linear. The direct values of $S_0(C)$ obtained by this last method are plotted in Fig. 4. The reasonable agreement of these results with the first ones allows us to confirm our above-mentioned conclusion that for relatively low concentrations (less than approximately 50%), the suspension is homogeneous but not random [experimental $S_0(C)$ differs from HD's one].

IV. VELOCITY FLUCTUATIONS

As the suspension is fluidized and no vortex-like convective motion could be detected at any concentration, the average velocity of any particle is equal to zero, and consequently its instantaneous velocity is also its velocity fluctuation.

A. Velocity fluctuations of a single particle

By collecting the velocities of the particles at different times, we get reliable statistics (more than 10^5) to compute the average amplitude of velocity fluctuation, or the spatial velocity correlation. The root of the standard deviation of the horizontal component and the vertical component of an individual particle velocity are equal, we denote it u_0, $u_0 = \delta u_i = \sqrt{(\mathbf{u_p} \cdot \mathbf{i} - \overline{\mathbf{u_p} \cdot \mathbf{i}})^2}$, where $\mathbf{i}$ is equal to the unit vector along the horizontal ($\mathbf{x}$) or the vertical ($\mathbf{z}$) direction, and $\mathbf{u_p}$ is the particle velocity vector. The value u_0 does not change when averaging on time or on the different particles, in agreement with the ergodic principle. u_0 is of the same order of mag-
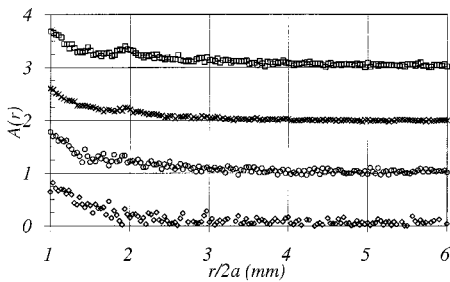
FIG. 7. Angular velocity correlation vs normalized distance for $C=13$ ($\times$), 25 ($\diamond$), 35 ($\bigcirc$), 46 ($\triangle$)%. For clarity the curves are shifted vertically by a constant value [note that $A(\infty)=0$ in all cases].

FIG. 8. Size dependence of the fluctuation of the mean velocity in a subvolume (πR^2). Log–log plot of $\Delta U_R/U_s$ vs R/a for $C=13$ ($\times$), 28 ($\diamond$), 40 ($\bigcirc$), 46 ($\triangle$)%. The dashed line has a -1 slope.

nitude as the inlet velocity U_d in the fluidized suspension, which is also of the same order as the sedimentation velocity (measured after switching off the flow rate). This velocity fluctuation u_0 scales with U_d, whatever the size of the suspension, the number of particles, and the value of Re, provided that it remains lower than 1. This is illustrated in Fig. 6 where the normalization of u_0 by U_d results in the merging of the different sets of data collected for different parameters of suspension, which means: two different values of the width of the cell (10 and 20 cm), two different Re numbers i.e., two different values for the solid density (aluminum and brass). We note that those normalized velocity fluctuations increase as the concentration increases up to a $C\sim 50\%$. For higher concentration, velocity fluctuations decrease, to reach a zero value at close packing. We have already studied the amplitude of this velocity fluctuation, especially their probability distribution function (PDF).[20] It appears that the PDF are direction and concentration dependent. Particularly, vertical PDF are asymmetric. This disymmetry increases as C increases, and, results in a rise of the probability of large upward velocities which penalizes the smaller ones. This anomalous behavior is in agreement with a hyperdiffusion measured along the vertical direction, associated with the appearance of rapid transient channel where particles are suddenly advected by fluid upflow.

B. Velocity spatial correlation

Individual particles' velocities are spatially correlated and concentration dependent. To avoid maximizing the influence of large upward velocities, we normalized our calculated spatial velocity correlation by the amplitude of the involved velocities, i.e., we calculate the mean cosine, $A(r)$, of the angle between the velocity vectors of the particles distant of r from each other,

$$A(r)=\langle\cos(\mathbf{u}(\mathbf{r_0}),\mathbf{u}(\mathbf{r_0}+\mathbf{r}))\rangle=\left\langle\frac{\mathbf{u}(\mathbf{r_0})\cdot\mathbf{u}(\mathbf{r_0}+\mathbf{r})}{\|\mathbf{u}(\mathbf{r_0})\|\|\mathbf{u}(\mathbf{r_0}+\mathbf{r})\|}\right\rangle.\tag{8}$$

$A(r)$ is plotted in Fig. 7 for four different concentrations. The velocities of contact particles are strongly correlated [$A(r=2a)\sim 0.7$] and the correlation extends to a length varying from two to three diameters for increasing concentrations. Note that from our 2-D study, the relevant normalization of the velocity correlation length remains ambiguous
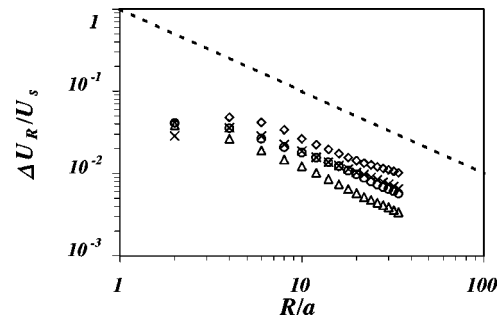
and can be either the particle size or the cell thickness. A peak of $A(r)$ at $r=4a$, hardly appearing at $C=35\%$ and more obvious at $C=46\%$, reflects the existence of translating contact triplets, and more generally, the presence of clusters in the suspension. On the other hand, the smooth decrease of $A(r)$ indicates that the clusters do not have any characteristic size.

C. Fluctuations of the mean velocity in a subvolume

In the same way that we measured N_R and ΔN_R, we can measure the mean velocity U_R in a disk of radius R by averaging the individual velocities of the particles inside this disk at a given time: $U_R=(1/N_R)\Sigma_{v_R}\mathbf{u}_p$. We have computed the velocity fluctuations ΔU_R as the root of the quadratic deviation of U_R, averaged on numerous identical subvolumes taken at different space and time: $\overline{\Delta U_R^2}=\overline{(U_R-\bar{U})^2}$ where $\bar{U}=0$ in our fluidized suspension. Figure 8 is a log–log plot of ΔU_R vs R. The velocity fluctuation dependence with R is nearly R^{-1}, whatever the concentration value.

This R^{-1} dependence of ΔU_R can be explained by an argument initially used by Hinch for a 3-D suspension[9] and here transposed to the 2-D case as follows: The velocity fluctuations ΔU_R can be related to fluctuation of the particle number ΔN_R from a balance between the buoyancy force on the disk and the sidewalls friction. For a disk of size R and
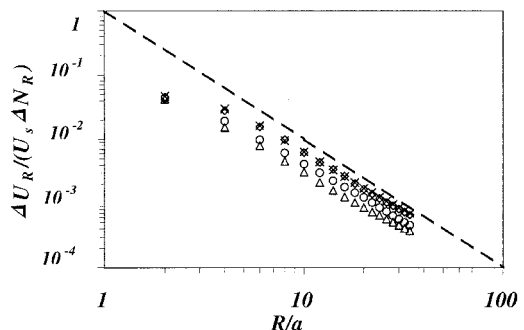

FIG. 9. Size dependence of the ratio of the velocity fluctuations to the density fluctuations in a subvolume. Log–log plot of $\Delta U_R/U_s\Delta N_R$ vs R/a for $C=13$ ($\times$), 28 ($\diamond$), 40 ($\bigcirc$), 46 ($\triangle$)%. The dashed line has a -2 slope.
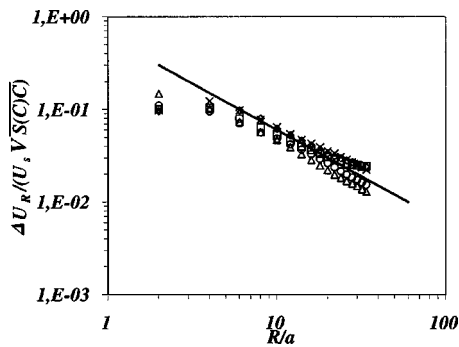
FIG. 10. Log–log plot of $\Delta U_R/U_s\sqrt{S_0(C)C}$ vs R/a for $C = 13\,(\times)$, $28\,(\diamond)$, $40\,(\bigcirc)$, $46\,(\triangle)\%$. The line through the data is the theoretical prediction $0.6a/R$.

thickness $b \sim a$, this friction force is of the order $\eta(\Delta U_R/a)R^2$ so that

$$\Delta U_R \sim U_s\left(\frac{a}{R}\right)^2 \Delta N_R. \tag{9}$$

Since ΔN_R is related to $\overline{N_R}$ [cf. Eq. (6)] and $C = \overline{N_R}a^2/R^2$, one finally gets

$$\frac{\Delta U_R}{U_s} \sim \sqrt{CS_0(C)}\,\frac{a}{R}, \tag{10}$$

hence an R^{-1} dependence which compare with the one observed in Fig. 8.

Furthermore, we can test the validity of the first step of the model: The extra buoyancy force associated with ΔN_R is balanced by an extra wall friction associated with ΔU_R. Equation (9) requires a dependence of $(\Delta U_R/\Delta N_R)$ as R^{-2}. Our data plotted in Fig. 9 are in reasonable agreement with the predicted dependence. Therefore, this supports the contention that the wall friction is the predominant viscous force in our system.

Regarding Eq. (10), we should be able to predict the amplitude of ΔU_R for various concentrations with the knowledge of $S_0(C)$. We plot in Fig. 10 the ratio of $\Delta U_R/U_s$ to $\sqrt{S_0(C)C}$ vs R. Almost all the data collapse around the full line $0.6a/R$ in agreement with Eq. (10). Thus, we find here an illustration of the influence of the structure factor on the amplitude of velocity fluctuation, and of the dependence of this structure factor with concentration. It has been demonstrated that the structure in our quasi-2-D suspension differs from a random one, hence it seems that in further studies, knowledge of the structure factor should be needed to correctly predict the dependence of velocity fluctuations with concentration. One could remark that this velocity fluctuation term ΔU_R is not the current one $\delta v_p = u_0$ measured in literature. From our data, we have calculated $u_0/(U_s\sqrt{S_0(C)C})$ for various parameters, and find that this value is always equal to 0.15 ± 0.05, for C lower than C^*. Using Fig. 10, we find that this value corresponds to the value of $\Delta U_R/(U_s\sqrt{S_0(C)C})$ for R of the order of 2–5a, which is approximately the velocity correlation length [c.f. Fig. 7]. This would mean that Hinch's approach can predict the velocity fluctuations δv_p by calculating ΔU_R for R of the order of the velocity correlation length.

V. CONCLUSION

We have reported on measurements of the structure, density, and velocity fluctuations of a quasi-2-D suspension of monodisperse particles. The pair distribution function and the long wavelength structure factor (measured either from the density distribution or the density fluctuations), reveal that the suspension microstructure is definitively not random and that the beads tend to be much more in contact than in a hard disk fluid. We have also measured the size dependence of the density and of the velocity fluctuations in a subvolume. To account for these dependencies, we have adapted Hinch's argument to our quasi-2-D suspension including the suspension microstructure and the wall friction. The agreement between experimental results and theoretical model is rather good, and then emphasizes the crucial roles played by the thickness of the vessel through wall friction and by the structure factor. The latter, which is definitively not random, will be a determinant input for further modeling and computing of macroscopic suspensions.

[1] J. M. Ham and G. M. Homsy, "Hindered settling and hydrodynamic dispersion in quiescent suspension," Int. J. Multiphase Flow **14**, 533 (1988).

[2] R. H. Davis and M. A. Hassen, "Spreading of the interface at the top of a slightly polydisperse sedimenting suspension," J. Fluid Mech. **196**, 107 (1988).

[3] J. Martin, N. Rakotomalala, and D. Salin, "Hydrodynamic dispersion of non-colloidal suspensions: Measurement from Einstein's argument," Phys. Rev. Lett. **74**, 1347 (1995).

[4] H. Nicolai, B. Herzhaft, E. J. Hinch, L. Oger, and E. Guazzelli, "Particle velocity fluctuations and hydrodynamic self-diffusion of sedimenting non-Brownian spheres," Phys. Fluids **7**, 12 (1995).

[5] A. J. C. Ladd, "Sedimenting of homogeneous suspensions of non-Brownian spheres," Phys. Fluids **9**, 491 (1997).

[6] P. N. Segre, E. Herbolzheimer, and P. M. Chaikin, "Long-range correlations in sedimentation," Phys. Rev. Lett. **79**, 2574 (1997).

[7] G. K. Batchelor, "Sedimentation in a dilute dispersion of spheres," J. Fluid Mech. **52**, 245 (1972).

[8] R. E. Caflisch and J. H. C. Luke, "Variance in sedimentation speed of a suspension," Phys. Fluids **28**, 759 (1985).

[9] E. J. Hinch, *Disorder and Mixing* (Kluwer Academic, Dordrecht, 1998), p. 153.

[10] D. Bruneau, F. Feuillebois, J. Blawzdziewick, and R. Anthore, "Three-dimensional intrinsic convection in dilute and dense dispersion of settling spheres," Phys. Fluids **10**, 55 (1998).

[11] J. Z. Xue, E. Herbolzheimer, M. A. Rutgers, W. B. Russel, and P. M. Chaikin, "Diffusion, dispersion and settling of hard spheres," Phys. Rev. Lett. **69**, 1715 (1992).

[12] H. Nicolai and E. Guazzelli, "Effect of the vessel size on the hydrodynamic diffusion of sedimenting spheres," Phys. Fluids **7**, 3 (1995).

[13] L. Talini, J. Leblond, and F. Feuillebois, "A pulse field gradient NMR technique for the determination of the structure of suspensions of non-Brownian particles with application to packings of spheres" J. Magn. Reson. **132**, 287 (1998).

[14] D. L. Koch and E. S. G. Shaqfeh, "Screening in sedimenting suspensions," J. Fluid Mech. **224**, 275 (1991).

[15] M. P. Brenner, "Screening mechanisms in sedimentation," Phys. Fluids **11**, 754 (1999).

[16] T. M. Truskett, S. Torquato, S. Sastry, P. G. Debenedetti, and F. H. Stillinger, Phys. Rev. E **58**, 3083 (1998).

[17] N. F. Carnahan and K. E. Stirling, "Equation of state for nonattracting rigid spheres," J. Chem. Phys. **51**, 635 (1969).

[18] M. Baus and J. L. Colot, "Thermodynamics and structure of a fluid of hard rods, disks, spheres or hyperspheres from rescaled virial expansion," Phys. Rev. A **36**, 3912 (1987).

[19] J. P. Hansen and I. R McDonald, *Theory of Simple Liquid* (Academic, New York, 1976).

[20] F. Rouyer, J. Martin, and D. Salin, "Non-Gaussian dynamics in quasi-2D noncolloidal suspensions," Phys. Rev. Lett. **83**, 1058 (1999).